CHEMISTRY OF MATERIALS

pubs.acs.org/cm
Article

Design and Processing as Ultrathin Films of a Sublimable Iron(II) Spin Crossover Material Exhibiting Efficient and Fast Light-Induced Spin Transition

Published as part of Chemistry of Materials virtual special issue "In Honor of Prof. Clement Sanchez".

Miguel Gavara-Edo, Francisco Javier Valverde-Muñoz, M. Carmen Muñoz, Safaa Elidrissi Moubtassim, Francisco Marques-Moros, Javier Herrero-Martín, Kateryna Znovjyak, Maksym Seredyuk,* José Antonio Real,* and Eugenio Coronado*

Cite This: *Chem. Mater.* 2023, 35, 9591−9602

ABSTRACT: Materials based on spin crossover (SCO) molecules have centered the attention in molecular magnetism for more than 40 years as they provide unique examples of multifunctional and stimuli-responsive materials, which can be then integrated into electronic devices to exploit their molecular bistability. This process often requires the preparation of thermally stable SCO molecules that can sublime and remain intact in contact with surfaces. However, the number of robust sublimable SCO molecules is still very scarce. Here, we report a novel example of this kind. It is based on a neutral iron(II) coordination complex formulated as $[Fe(neoim)_2]$, where neoimH is the ionogenic ligand 2-(1*H*-imidazol-2-yl)-9-methyl-1,10-phenanthroline. In the first part, a comprehensive study, which covers the synthesis and magnetostructural characterization of the $[Fe(neoim)_2]$ complex as a bulk microcrystalline material, is reported. Then, in the second part, we investigate the suitability of this material to form thin films through high-vacuum sublimation. Finally, the retainment of all present SCO capabilities in the bulk when the material is processed is thoroughly studied by means of X-ray absorption spectroscopy. In particular, a very efficient and fast light-induced spin transition (LIESST effect) has been observed, even for ultrathin films of 15 nm.

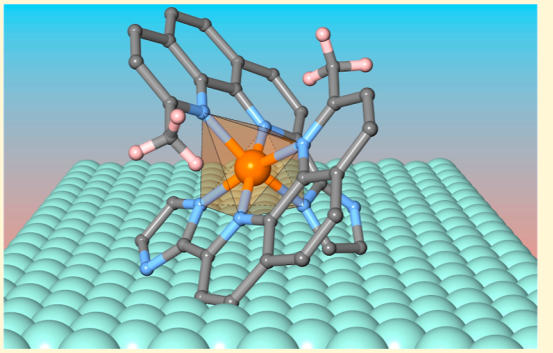

KEYWORDS: *spin-crossover, Fe(II) complexes, sublimation, LIESST, thin films*

INTRODUCTION

In hexacoordinated iron(II) spin crossover (SCO) complexes, the energy gap between the so-called low-spin (LS, $t_{2g}^6e_g^0$) and high-spin (HS, $t_{2g}^4e_g^2$) states is on the order of magnitude of the thermal energy. This fact confers electronic lability to these materials[1−4] and, consequently, a LS ↔ HS spin switching can be triggered by applying various external stimuli such as temperature or pressure changes, light irradiation, and electric fields and even by host−guest interactions.[5−9] Due to the antibonding nature of the e_g orbitals, the spin transition from LS to HS is accompanied by changes in the size and shape of the SCO active coordination centers, often leading to a significant expansion of the crystal lattice (by ca. 10%). Depending on the structural nature of the complex, these changes can spread over the crystals in a cooperative way, leading to a thermal hysteresis and thus to memory effects, which are reflected in the magnetic, calorimetric, optical, and even electrical properties of the material.[1−9] These unique characteristics have made iron(II) SCO complexes a relevant class of molecule-based switchable materials with potential use as device components for applications in fields such as molecular electronics and spintronics. Still, to achieve this end, it is necessary to process these SCO materials at the nanoscale.[10−13]

Among the available strategies, high-vacuum (HV) sublimation has been demonstrated to be an excellent methodology to prepare (ultra)thin films of SCO molecules.[11] The most prolific family of sublimable iron(II) SCO complexes is constituted of pyrazolylborate-based anionic ligands, such as hydro-trispyrazolylborate ($[HB(pz)_3]^-$) and its −3,5-dimethylpyrazolyl homologue ($[HB(3,5\text{-}pz)_3]^-$)[14,15] or, more recently, hydrotris(triazolyl)borate ($[HB(trz)_3]^-$)[14,16] and dihydropyrazolylpyridylpirazoleborate ($[H_2B(pz)(pzpy]^-$)

Received: July 7, 2023
Revised: October 17, 2023
Accepted: October 18, 2023
Published: November 13, 2023

Scheme 1. Tridentate and Bidentate Negatively Charged Ligands (L) of the Pyrazolylborate-Type and Other Meridional-Type Ones and the Ancillary Chelate Bidentate α-Diimine Ligands (L′) Used in Combination with $[H_2B(pz)_2]^-$ One

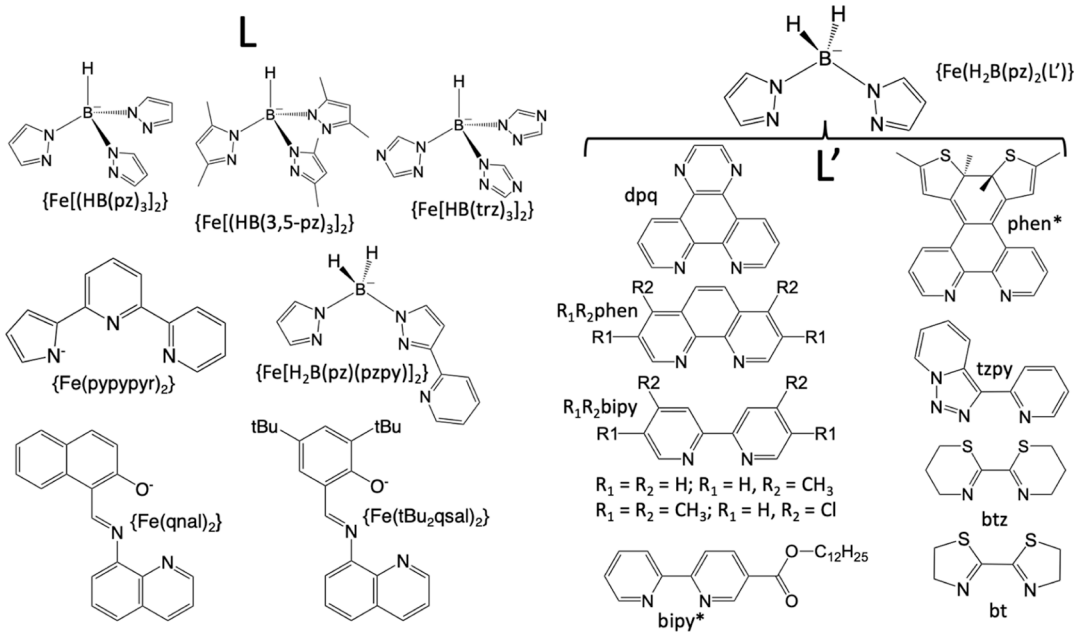

Scheme 2. Simplified Scheme of the Pathway Followed to Afford the $[Fe(neoim)_2]$ Complex

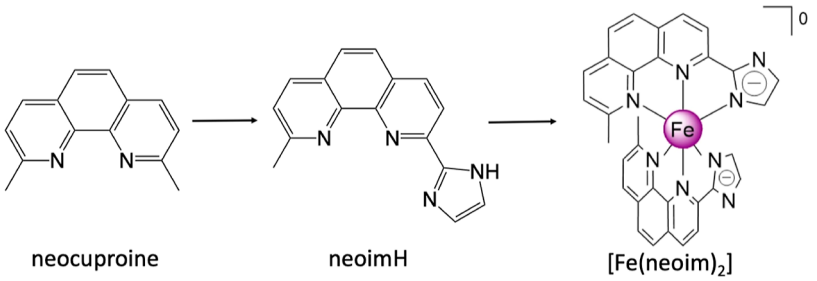

(Scheme 1).[17] The tridentate nature and negative charge of these particular ligands afford neutral homoleptic $[FeL_2]$ SCO complexes. Except for ($[H_2B(pz)(pzpy]^-$), which is a meridional tridentate ligand, all of them act as facial ones. Still, there are a few other meridional tridentate ones not based on pyrazolylborate, such as ($[pypypyr]^-$), ($[qnal]^-$), and ($[tBu_2qsal]^-$).[18−20] In contrast, the use of the bidentate dihydrobispyrazolylborate ($[H_2B(pz)_2]^-$) ligand introduces a degree of freedom to the system, generating a rich variety of $[Fe(H_2B(pz)_2)_2(L')]$ heteroleptic SCO complexes, being L′ chelate bidentate α-diimine ligands derived from either 1,10-phenanthroline or 2,2′-bipy[21−27] and other related such as tzpy, btz, and bt (Scheme 1).[28] Also, few additional SCO complexes have also been selected to assess their suitability as sublimable materials.[29−34]

Studying the thermal stability of these compounds as well as the retainment of their switchable SCO properties once deposited as ultrathin films by sublimation or even as isolated molecules on different types of surfaces has become a growing research activity in the last 10 years,[20,24,26−28,35−44] as recently reviewed.[45,46] Despite this, only very few sublimable Fe(II) SCO molecules being robust enough to maintain their integrity when integrated in electronic devices are reported.[47] Even more, only one molecule has shown, so far, a clear electrical reading of both thermal- and light-induced spin transitions.[41,48] Here, we report the synthesis, processing as thin films, and characterization of a novel neutral iron(II) coordination complex formulated as $[Fe(neoim)_2]$, where neoimH is the ionogenic ligand 2-(1*H*-imidazol-2-yl)-9-methyl-1,10-phenanthroline (see Scheme 2). In bulk, this molecular complex exhibits both thermal- and light-induced spin transitions. These properties are retained when the complex is deposited as thin films by sublimation, as shown by means of X-ray absorption spectroscopy. The results demonstrate the strong thermal stability of this molecular complex. Additionally, the study evidences an outstandingly fast and effective sensitivity of these films toward both visible and X-ray light-induced LS to HS conversions, which is highly appealing for posterior integration as ultrathin films in a first generation of spintronic devices that can be addressed by light.

RESULTS AND DISCUSSION

Synthesis. The new neutral SCO complex $[Fe(neoim)_2]$ results from the design of ionogenic robust ligands based on 1,10-phenanthroline since this function typically offers the appropriate ligand field strength to favor thermal spin-state conversion in the iron(II) ion. To obtain this complex, we functionalized the neocuproine ligand (2,9-dimethyl-1,10 phenanthroline) with a complementary imidazole function, thereby affording the novel tridentate ligand 2-(1*H*-imidazol-2-yl)-9-methyl-1,10-phenanthroline (hereafter neoimH). Then,

https://doi.org/10.1021/acs.chemmater.3c01704
Chem. Mater. 2023, 35, 9591−9602

upon deprotonation in the presence of iron(II), we obtained $[Fe(neoim)_2]$ (see Scheme 2 and Methods sections for details). This compound was first dried under an Ar flow at 440 K for 12 h to afford an unsolvated green-brown colored powder. Upon recrystallization by slow diffusion of hexane vapors into a solution of the molecular complex in chloroform, dark-green single crystals of the solvate $[Fe(neoim)_2]\cdot H_2O\cdot 2CHCl_3$ were next obtained. Nonetheless, collected IR spectra of both solvated and unsolvated forms were essentially identical, the main difference being the intense band at 746 cm^{-1}, which corresponds to the C−Cl stretching band of the $CHCl_3$ solvent (Figure S1). Additionally, the loss of solvents was observed to induce noticeable changes in the crystal packing of both forms (Figure S2). Regarding the thermal stability of the molecule, thermogravimetric analysis showed that the unsolvated samples endure temperatures up to ca. 600 K (Figure S3), indicating large thermal stability and hinting at its potential sublimability.

Structure. The crystal structure of $[Fe(neoim)_2]\cdot H_2O\cdot 2CHCl_3$ was solved at 120 K (Table S1 contains relevant crystallographic information). The unit cell corresponds to the chiral orthorhombic $P2_12_12_1$ space group. Table 1 contains a selection of relevant Fe−N bond lengths and angles. The iron(II) center is at the center of a distorted $[FeN_6]$ octahedral coordination environment generated by the two tridentate $[neoim]^-$ ligands. These are orthogonally oriented (89.89°) to each other around the iron(II) center (Figure 1). The average ⟨Fe−N⟩ bond length, equal to 1.969(8) Å, is characteristic of the LS state; however, the sum of the deviation from 90° of the 12 "cis" N−Fe−N angles, $\Sigma = (|\theta - 90|) = 83.6°$, is significantly high but consistent with the geometric constraints induced by the tridentate nature of the ligand.

Table 1. Selected Bond Lengths (Å) and Angles (deg) of $[Fe(neoim)_2]\cdot H_2O\cdot 2CHCl_3$

bond lengths		bond angles	
Fe−N1	2.047(7)	N2 Fe N1	80.9(3)
Fe−N2	1.883(9)	N3 Fe N1	160.9(4)
Fe−N3	1.968(8)	N5 Fe N1	92.9(3)
Fe−N5	2.051(8)	N6 Fe N1	105.3(3)
Fe−N6	1.883(8)	N7 Fe N1	89.5(3)
Fe−N7	1.983(8)	N2 Fe N3	80.0(3)
⟨Fe−N⟩	**1.969(8)**	N2 Fe N5	105.2(3)
		N6 Fe N2	171.1
		N2 Fe N7	94.1(3)
		N3 Fe N5	91.7(3)
		N6 Fe N3	93.7(3)
		N7 Fe N3	92.1(3)
		N6 Fe N5	81.1(3)
		N7 Fe N5	160.8(4)
		N6 Fe N7	79.9(3)
		$\Sigma = (|\theta - 90|)$	**83.6**

Regarding the crystal packing of the complexes (Figure 2), a perfect superposition between them is found along the *a*-direction defining columns. However, along the *b* and *c* directions, remarkably short intermolecular contacts are found. In particular, atoms C3 and C4 of the phenanthroline moiety of a molecule act as a wedge, filling the dihedral space generated between the imidazole and phenanthroline moieties of the adjacent complex and defining contacts well below the sum of the van der Waals radii [d(C3···C16) = 3.299 Å, d(C4···C21) = 3.193 Å] in addition to d(C31···C19) = 3.444 Å], which extend along the *b* direction defining supramolecular chains. These chains are packed along *c* in such a way that short interchain contacts [d(C31···C24) = 3.437 Å, d(C31···C27) = 3.427 Å, and d(C32···C27) = 3.362 Å] alternate with wide hexagonal channels running along *a* where the solvent molecules are located. The water molecule interacts via hydrogen bonding with one of the two chloroform molecules [d(C34···O1) = 3.092, angle C34−H···O1 = 174.67°) and also interacts with the C23 atom belonging to the phenanthroline moiety [d(O1···C7) = 3.371 Å]. In addition, C11 of this moiety has short contact with Cl3 of the other chloroform molecule.

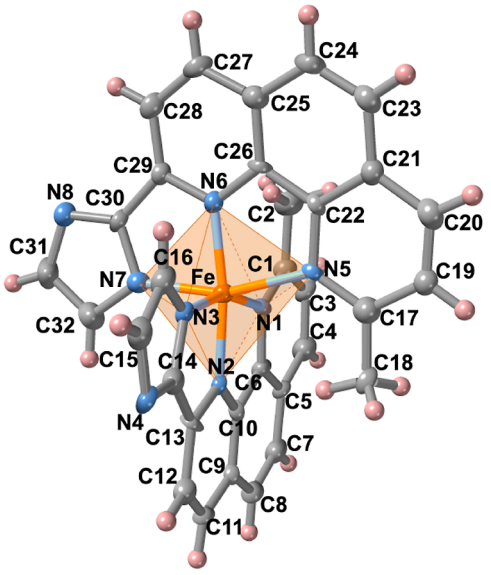

Figure 1. Molecular structure of compound $[Fe(neoim)_2]\cdot H_2O\cdot 2CHCl_3$.

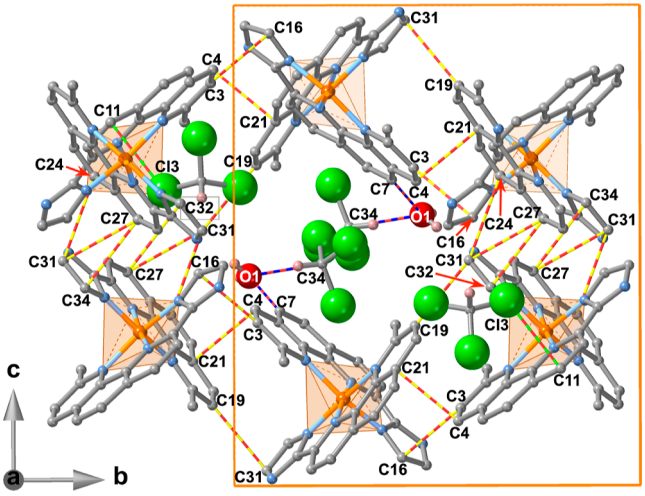

Figure 2. Representative crystal packing of $[Fe(neoim)_2]\cdot H_2O\cdot 2CHCl_3$. Thin bicolor rods represent intermolecular short contacts. The hydrogen atoms of the complex were omitted for clarity.

Magnetic Properties. The magnetic properties of $[Fe(neoim)_2]\cdot H_2O\cdot 2CHCl_3$ crystals and the corresponding desolvated form ($[Fe(neoim)_2]$) are displayed in Figure 3 as the thermal dependence of the $\chi_M T$ product, where χ_M is the magnetic molar susceptibility and T is the temperature. For the

https://doi.org/10.1021/acs.chemmater.3c01704
Chem. Mater. 2023, 35, 9591−9602

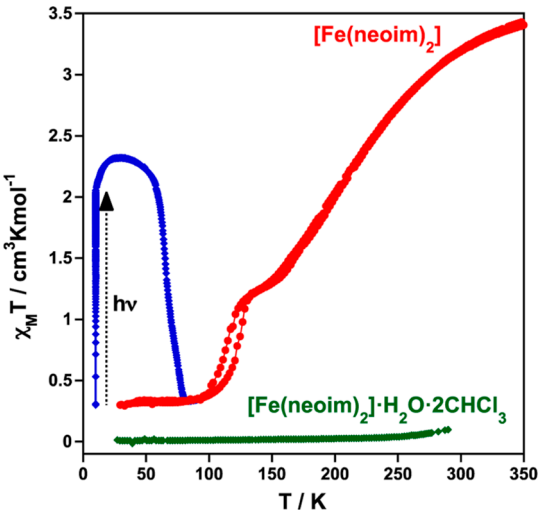

Figure 3. Magnetic properties of $[Fe(neoim)_2]\cdot H_2O\cdot 2CHCl_3$ and its desolvated form.

solvated form, the $\chi_M T$ value is constant and around 0.1 cm^3 K mol^{-1} in the whole temperature range, indicating that this material is essentially in the diamagnetic LS state. The loss of the solvent molecules provokes a dramatic change in the magnetic properties, which exhibit a spin transition. Thus, at 390 K, the $\chi_M T$ product shows a value of ca. 3.49 cm^3 K mol^{-1}, consistent with a HS state. Upon cooling, $\chi_M T$ decreases very gradually down to ca. 1.28 cm^3 K mol^{-1} at ca. 148 K. Upon further cooling, in the interval 148−132 K, the slope of the $\chi_M T$ vs T plot increases significantly, delineating an inclined short step followed by a steeper $\chi_M T$ vs T dependence until reaching a value of ca. 0.30 cm^3 K mol^{-1} at 80 K that stays constant down to the lowest temperature investigated and indicates that most of the iron(II) centers are in a LS state. This second step exhibits an ca. 8 K wide hysteresis loop upon heating.

Photogeneration of the metastable HS* state from the LS state—the so-called light-induced excited spin state trapping (LIESST)[49] effect—was carried out at 10 K, irradiating the desolvated powder with green light (λ = 532 nm, 11.2 mW). Thus, $\chi_M T$ increases saturating to a value ca. 2.0 cm^3 K mol^{-1} in 15 min, which, considering the "high" characteristic temperature of the thermal SCO (50 % HS to LS conversion is reached at about 200 K) and the penetration depth of the laser through the powder sample, is noticeably fast and

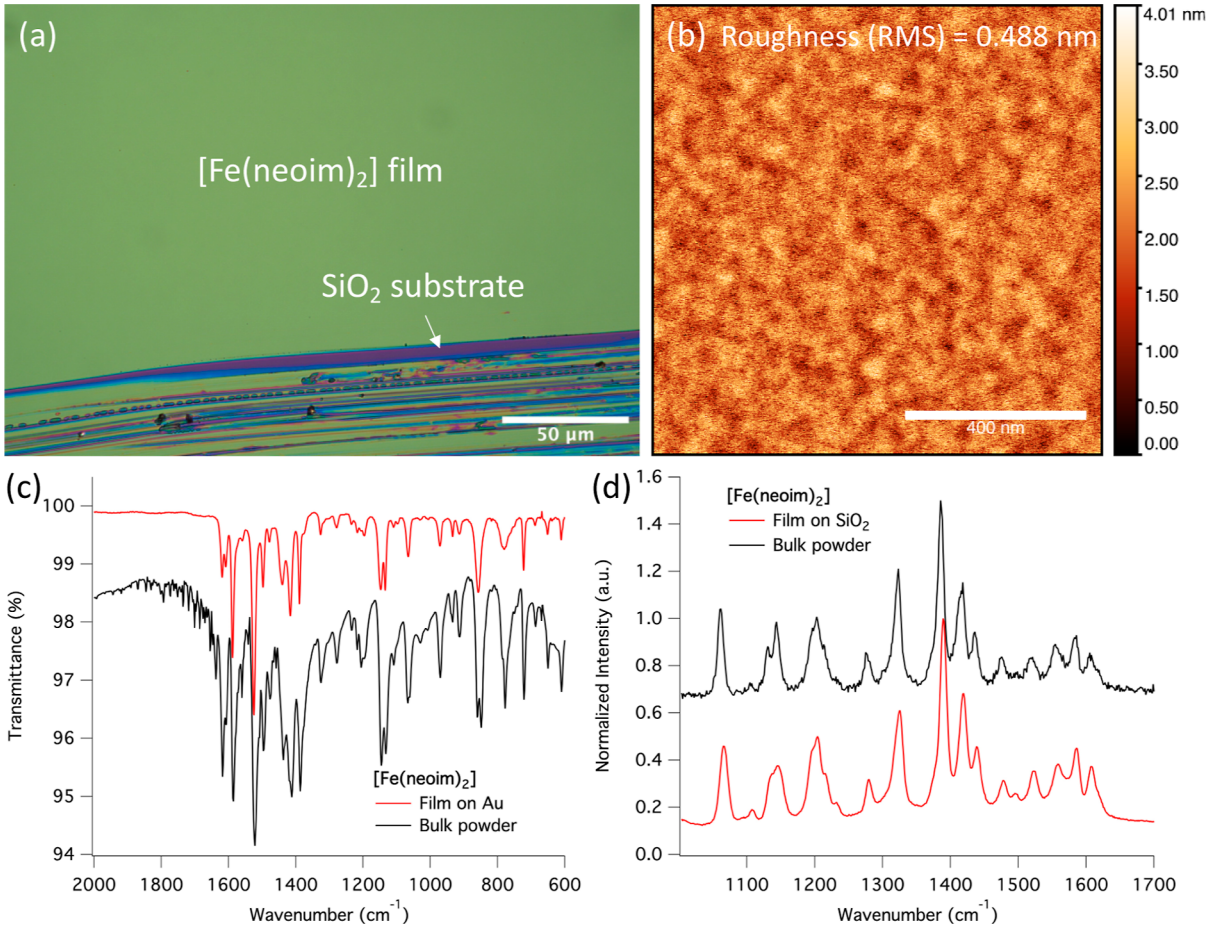

Figure 4. (a) OM image of a 100 nm thick $[Fe(neoim)_2]$ film (green area) deposited on a SiO_2 substrate (purple area). (b) AFM image of a 1 μm × 1 μm region collected on the same film, indicated in (a). (c) IR spectra of a 100 nm thick $[Fe(neoim)_2]$ film deposited on a Au substrate (red line) and of the bulk powder reference (black line). (d) Raman spectra of a 100 nm thick $[Fe(neoim)_2]$ film deposited on a SiO_2 substrate (red line) and of the bulk powder reference (black line). In (a,b), the scales are 50 μm and 400 nm, respectively. At the bottom part of (a), the rough area corresponds to a manually performed scratch to show the underlying substrate. In (b), the roughness of the film calculated as the rms value is indicated.

https://doi.org/10.1021/acs.chemmater.3c01704
Chem. Mater. 2023, 35, 9591−9602

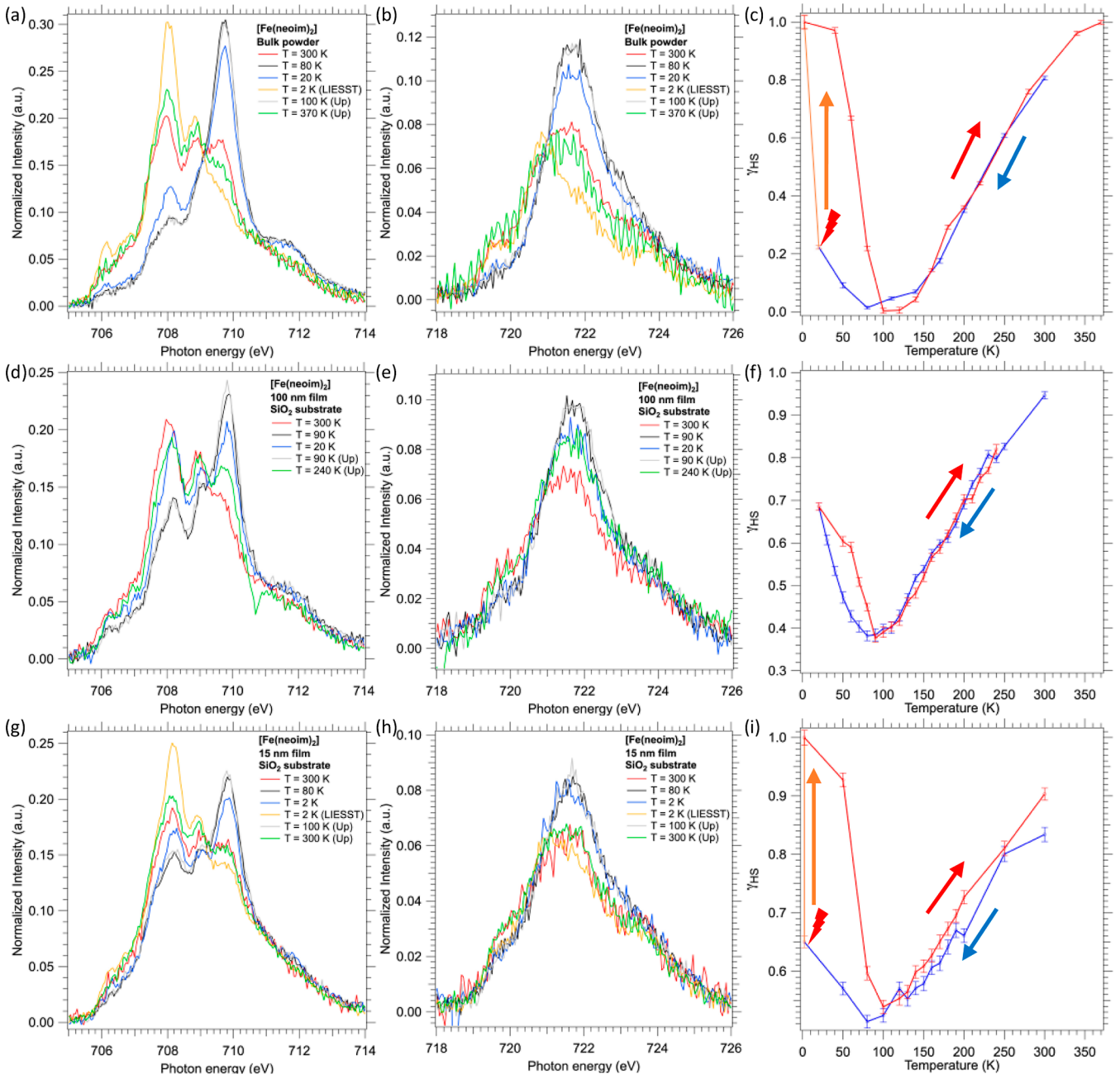

Figure 5. XAS spectra collected at 300, 80, and 20 K during cooling, 2 K after 10 min of red laser irradiation, and at 100 and 370 K during heating in the Fe (a) L_3 and (b) L_2 edges for $[Fe(neoim)_2]$ scattered on C-tape and (c) calculated HS fraction from each XAS spectrum collected at each temperature along the full thermal cycle (blue line—cooling, orange line—LIESST and red line—heating). XAS spectra collected at 300, 90, and 20 K during cooling and at 90 and 240 K during heating in the Fe (d) L_3 and (e) L_2 edges for a 100 nm thick film of $[Fe(neoim)_2]$ deposited on SiO_2 and (f) the calculated HS fraction from each XAS spectrum collected at each temperature along the full thermal cycle (blue line—cooling and red line—heating). XAS spectra collected at 300, 80, and 2 K during cooling, at 2 K after 10 min of red laser irradiation, and at 100 and 300 K during heating in the Fe (g) L_3 and (h) L_2 edges for a 15 nm thick film of $[Fe(neoim)_2]$ deposited on SiO_2 and (i) the calculated HS fraction from each XAS spectrum collected at each temperature along the full thermal cycle (blue line—cooling, orange line—LIESST and red line—heating).

efficient. After switching off the light and heating the system at a rate of 0.3 K min^{-1}, a gradual increase of $\chi_M T$ is induced that attains a maximum value of 2.32 cm^3 K mol^{-1} in the interval of 22−38 K. This small additional raise in $\chi_M T$ reflects the thermal population of different microstates originated from the zero-field splitting of the HS* state and corresponds to a population of the HS state ca. 66.5%. Above 38 K, $\chi_M T$ decreases until joining the thermal SCO curve at ca. 80 K, indicating that the metastable HS* state has thermally relaxed back to the stable LS state. The corresponding T_{LIESST} temperature, evaluated as $\delta(\chi_M T)/\delta T$,[2] is ca. 65 K. This temperature is consistent with the inverse-energy-gap law, i.e., the metastability of the photogenerated HS* species decreases as the stability of the LS increases.[50−53]

Highly Homogeneous Thin Films of $[Fe(neoim)_2]$. $[Fe(neoim)_2]$ was sublimed under UHV conditions following a similar protocol used by us for other SCO molecules.[28,41] At this respect, ca. 100 mg of the desolvated bulk powder is

https://doi.org/10.1021/acs.chemmater.3c01704
Chem. Mater. 2023, 35, 9591−9602

loaded inside the Knudsen cell fitting our molecular beam epitaxy evaporation chamber (customized CREATEC system within a clean room class 10,000) and preconditioned by means of a smooth heating up to 120 °C for degassing. The sublimation conditions consist in heating the material at 245 °C in a vacuum pressure of ca. 5×10^{-8} mbar to reach a constant deposition rate of ca. 0.4 Å·s^{-1}, as monitored with a calibrated quartz crystal microbalance located next to the deposition substrate. Different films were grown in the range of 15−150 nm thickness, verified with nanometric resolution via profilometry. The appearance and topography of these films were characterized by using optical microscopy (OM) and atomic force microscopy (AFM). The results from both microscopies show extremely homogeneous coverages of the substrates (Figure 4a,b), featured by the lack of distinguishable crystal grains and by very low roughness [ca. 0.5 nm calculated as the root-mean-square (rms) value using Gwyddion program). No diffraction peaks can be observed by means of the surface X-ray diffraction technique, indicating a highly amorphous character of the molecular films.

Regarding the chemical integrity, the composition of the thin films was determined via IR and Raman spectroscopies and compared to that of the bulk (Figure 4c,d). Two 100 nm thick films were separately grown using the same sublimation procedure; one was deposited on a Au-covered glass substrate destined for IR spectroscopy, and the other was deposited on a SiO_2 substrate for Raman spectroscopy. The collected IR spectrum of this film shows good matching with that obtained for the bulk powder between 2000 and 600 cm^{-1} (Figure 4c). The only noticeable differentiating feature comes from the presence of a very small fraction of remnant water molecules within the bulk powder, evidenced by the presence of a noisy band at about 1600 cm^{-1}. Regarding the Raman spectra, the resulting data show perfect matching between both film and bulk powder in the 1000−1700 cm^{-1} region. Interestingly, no laser damage was observed during this characterization on either sample despite using a highly energetic laser (473 nm—blue, power ca. 1.08 mW·μm^{-2}). This result further evidences the good stability of this molecular SCO material. Overall, both techniques prove the retainment of the chemical integrity of the molecular complex when sublimed as a thin film.

Spin-Crossover Properties of the [Fe(neoim)$_2$] Thin Films. The SCO behavior of different films was studied by means of the X-ray absorption spectroscopy (XAS) technique focused at the Fe $L_{2,3}$ edges. Thus, XAS spectra were collected for each film at different temperatures to respectively determine the electronic configuration (spin state) of their conforming molecules. At the same time, the bulk material was characterized in order to get reliable referential spectra and to provide a direct correlation tool to estimate the HS fraction present in each sample at each temperature. Last but not least, the LIESST effect was additionally studied for the bulk material and the thinnest film prepared (15 nm thick) by irradiating each of them, respectively, at 2 K for 10 min with a red laser (633 nm, 12 mW) and subsequently collecting their respective XAS spectra. Notice that the laser power indicated corresponds to the output full power. However, the laser beam must travel through an optical window and over a 50 cm distance within the HV chamber before reaching the film surface. Thus, the real power of the laser at the sample surface must be substantially lower compared to the output one, but it cannot be determined due to technical difficulties (see Methods). The XAS results for all samples are shown in Figure 5.

To characterize the bulk material, spectra were collected at different temperatures by first performing cooling from room temperature (300 K) to 2 K and then subsequent heating up to 370 K. As it can be observed in Figure 5a,b (red line), the initial state detected at 300 K can be assigned to a mixed HS−LS state where the HS one is predominant. This is characterized by the presence of both the most characteristic peaks of the HS state at the Fe L_3 edge (ca. 708.0 and 708.9 eV, respectively) and the most intense peak of the LS state (ca. 709.7 eV). Upon cooling to 80 K, a clear progressive change is observed consisting of a decrease in the intensity of the aforementioned HS state peaks at the Fe L_3 edge counterparted by an increase in intensity of the LS one (Figure 5a, black line). These observations, along with the typical increase in intensity of the main peak of the Fe L_2 edge, appearing around 721 eV (Figure 5b, black line), are consistent with the thermal HS to LS conversion of the material characterized by magnetic susceptibility measurements. However, a deviation in such a trend is observed upon further cooling. Particularly, the spectra collected down to 20 K show the progressive reversion of the spin state of the material toward a higher HS state fraction (Figure 5a,b, blue line). This behavior is typical of a soft X-ray-induced excited spin state trapping (SOXIESST) effect that photoexcites the material from LS to a metastable HS* state during the spectra collection.[54−59] In fact, despite the precautions taken regarding the use of a photon flux as low as possible in this beamline, as performed in previous experiments on other sublimable SCO molecules,[28,41] the effect on the bulk [Fe(neoim)$_2$] molecule seems outstandingly effective. Thus, we next decided to cool further to 2 K and irradiate with a red laser to investigate the LIESST effect as well with this technique. Interestingly, an almost full HS state spectrum is achieved only after 10 min of irradiation (Figure 5a,b, orange line). Noticeably, apart from confirming the LIESST effect observed in magnetic susceptibility measurements, this result further evidences the high susceptibility of this material toward light-induced SCO phenomena. Subsequently, the reversibility of these observed SCO-related behaviors were studied upon heating up to 370 K. Two different trends can be distinguished: first, a thermal relaxation of both SOXIESST and LIESST effects is observed, with the full LS state recovered at ca. 100 K (Figure 5a,b, gray line); second, upon further heating, the expected progressive conversion from LS to an almost full HS state at 370 K occurs (Figure 5a,b, green line). In order to facilitate the visualization of all these changes, we estimated the temperature dependence of the HS fraction by fitting each collected spectrum to a linear combination of the "full" HS and LS states spectra (collected at 80 and 370 K, respectively) (Figure 5c). In this plot, the different phenomenologies aforementioned are clearly monitored and quantified. For instance, at room temperature, the bulk material presents a HS fraction of ca. 80%, which fully converts to the LS state at ca. 80 K; below this temperature, the SOXIESST effect induces an overall HS fraction increase of ca. 20% down to 20 K; finally, a complete LIESST effect is reached after 10 min of red laser irradiation at 2 K.

The XAS characterization of the sublimed thin films with three different thicknesses (100, 150, and 15 nm) is plotted in Figures 5d−i and S4. The 100 nm film was subjected to cooling between 300 and 20 K followed by heating to 240 K

https://doi.org/10.1021/acs.chemmater.3c01704
Chem. Mater. 2023, 35, 9591−9602

(Figure 5d−f). The results obtained closely resemble those attained for the bulk material, exhibiting a large HS fraction (ca. 95%) at room temperature, which decreases down to ca. 37% at ca. 80 K. Then, at lower T, the clear SOXIESST effect is observed, reaching an outstandingly high HS fraction of ca. 68% at 20 K (Figure 5f) despite using a very low photon flux, same as that for the bulk powder (0.026 nA—ca. 4×10^{10} photons·s^{-1}·mm^{-2}). Finally, the completion of the SOXIESST effect's thermal relaxation is accomplished at 90 K upon heating. With respect to the remnant HS fraction of molecules at 80 K in the film, a plausible explanation is a slight shifting to lower temperatures of the spin transition as compared to the bulk powder, which is typically found for different sublimed films of SCO molecules.[39,60,61] This is subsequently accompanied by a larger presence of the SOXIESST effect at these temperatures that does not allow the spin transition completion.

Since the SOXIESST effect was very strong in this first sample and suspecting that the thermal SCO transition of the film might be more complete in the absence of this phenomenon, a second sample with similar thickness (150 nm) was also studied upon a photon flux reduction (Figure S4). Unfortunately, given the loss of spectra quality accompanying this protocol, only a small decrease in this parameter was achieved (ca. 0.020 nA compared to 0.026 nA). Still, the SOXIESST effect emerged below 80 K (Figure S4c) and the overall behavior showed the same trend as for the first film but with noisier spectra. Consequently, the sample was not studied in further detail.

A last experiment was performed on a very thin film (15 nm) with the aim of investigating the effect of such miniaturization on SCO behavior. Interestingly, the main SCO features are retained in this thin film (Figure 5g−i) including a SOXIESST effect below 80 K and an outstandingly effective LIESST effect. Due to the also very effective SOXIESST effect, this film shows a more incomplete thermal SCO transition than the thicker ones, although the presence of a larger pinned fraction of molecules in the HS state in the 15 nm film could also contribute to this observation, given its larger surface-to-volume fraction.[62,63] As far as the LIESST effect is concerned, a full HS state is reached within the 10 min irradiation period. This remarkable result on this 15 nm film, together with the amorphous and highly homogeneous nature of the films of [Fe(neoim)$_2$], evidence the high suitability of the material to exploit its light-induced switchability in spintronic devices. In fact, one of the open goals in this area is that of fabricating multifunctional spin valve devices in which the transport properties can be tuned not only by applying a magnetic field but also by light irradiation. The reason why this goal has not been achieved so far is twofold. On the one hand, it is due to the difficulty in preparing homogeneous ultrathin films from SCO molecules fulfilling the requirements of a spintronic vertical device: spin transport through the film while, upon thinning, avoiding the presence of shorts and retaining the SCO features of the molecules. At this respect, so far, only few vertical electronic devices have been fabricated, mostly integrating thin layers of SCO molecules belonging to the [Fe(H$_2$B(pz)$_2$)$_2$(L′)] family,[64−66] which typically display the LIESST effect and grow as homogeneous and amorphous films and whose first layer of molecules is known to sometimes decompose on metal surfaces of conventional electrodes.[26−28,37,60,67−73] Moreover, these devices have generally presented high limitations for electrically reading out the SCO behaviors due to the strongly insulating character of the molecules and, in relation to this, have presented low cyclability given the high voltages required, and the molecules' reactivity.[64−66] On the other hand, a further limitation that has been preventing the use of LIESST in spintronic devices is that only one example of a sublimable SCO molecule has been reported that exhibits an efficient and effective LIESST effect electrical response within an integrated electronic device.[41] Accordingly, it accomplishes a full photoexcitation in minutes, yet, unfortunately, the grown films of this material present high roughness and are composed of crystallites of ca. 50 nm, thus preventing its integration as ultrathin films in vertical devices.

CONCLUSIONS

Herein, we have reported a novel example of sublimable SCO material exhibiting extraordinary light-induced spin transition properties, which have been preserved when going from the bulk material to thin films. This robustness has been accomplished departing from the chemical design of a novel ionogenic tridentate ligand (neoim) that affords the new neutral complex [Fe(neoim)$_2$]. The desolvated form of this complex displays a very progressive thermal SCO transition ranging from 80 to 390 K, but more importantly, it experiences a quantitative and fast light-induced spin transition (LIESST effect). The sublimation of this material yields the formation of remarkably homogeneous and amorphous thin films in the range of 15−150 nm whose chemical integrity is identical to that of the bulk material. The SCO properties of these films were determined by XAS measurements. These studies indicate that in terms of both thermal- and light-induced spin transitions, the behavior of these films matches very well with that of the bulk powder. Thus, the thermal SCO behavior of the bulk material is well-preserved to a large extent in the films. More importantly, the LIESST effect is found to occur well in both bulk and thin films. Remarkably, the retention of such a phenomenon in the ultrathin films makes this material highly appealing for its implementation in applications such as electronic and spintronic devices. In fact, such a phenomenon has been so far poorly exploited in the field of molecular electronics[41,47,48,64] since not many SCO materials display it, especially in the case of sublimable ones, and their performance is generally not very outstanding in terms of quickness and effectiveness. In spintronic devices, such a phenomenon has not been exploited yet. In this regard, the novelty of the SCO molecule reported in this work is its high sensitivity to the LIESST effect that allows for achieving a virtually 100% yield in the photoinduced LS to HS state in less than 10 min of light irradiation. Hence, this feature, together with the high sublimation temperature and robustness of the molecule, makes this material an excellent candidate for its implementation in horizontal electronic devices integrating these SCO molecules with conducting/semiconducting 2D materials,[28,41,48,74−78] as well as in a first generation of light-addressable vertical spintronic devices in which the SCO ultrathin film is encapsulated in between two ferromagnetic electrodes.

METHODS

Synthesis. Iron(II) tetrafluoroborate hexahydrate, MnO_2, glyoxal, NH_3, and solvents were obtained from commercial sources and used as received without further purification. The sequence for synthesizing the ligand neoim and the corresponding iron(II) complex involves the successive synthesis of 9-methyl-1,10-phenanthroline-2-carbaldehyde

https://doi.org/10.1021/acs.chemmater.3c01704
Chem. Mater. 2023, 35, 9591−9602

(**B**), the ligand neoimH (**C**), and the complex [Fe(neoim)$_2$] (**D**), as depicted in the following scheme:

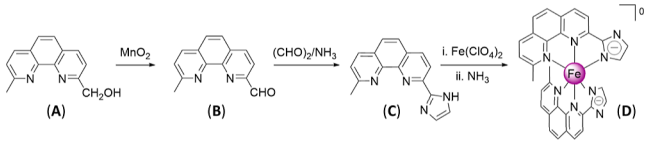

9-Methyl-1,10-phenanthroline-2-carbaldehyde (B). To (9-methyl-1,10-phenanthrolin-2-yl)methanol (**A**) (10 g, 44 mmol)[79] dissolved in *i*-PrOH (200 mL), active MnO_2 (20 g) was added. The reaction mixture was refluxed under stirring for 2 h and then, after cooling, filtered through a layer of Celite. The inorganic MnO_2 cake was twice washed by boiling *i*-PrOH (in portions of 50 mL each). The organic solution was evaporated to dryness. The resulting yellow−brown residue was purified by column chromatography on silica gel using $CHCl_3$ as the eluent. The intense white opaque band was collected. The yield of the target compound was about 5.0 g (51%). ^{1}H NMR (300 MHz, $CDCl_3$): δ 10.47 (1H, s, CHO), 8.32 (1H, dd, J^1 = 0.7 Hz, J^2 = 8.3 Hz, CH^7), 8.19 (1H, d, J = 8.2 Hz, CH^4), 8.11 (1H, d, J = 8.3 Hz, CH^8), 7.84 (1H, d, J = 8.8 Hz, CH^5), 7.73 (1H, d, J = 8.8 Hz, CH^6), 7.52 (1H, d, J = 8.2 Hz, CH^3), 2.92 (3H, s, Me). ^{13}C NMR (100 MHz, $CDCl_3$): δ 193.99, 160.50, 152.04, 145.70, 145.48, 137.48, 136.58, 131.29, 129.40, 127.13, 125.24, 124.43, 119.52, 25.94. Anal. Calcd for $C_{14}H_{10}N_2O$: C, 75.66; H, 4.54; N, 12.60. Found: C, 75.78; H, 4.35; N, 12.57.

2-(1*H*-Imidazol-2-yl)-9-methyl-1,10-phenanthroline (neoimH) (C). To a solution of 9-methyl-1,10-phenanthroline-2-carbaldehyde (5.0 g, 22 mmol) in EtOH (10 mL), aqueous glyoxal, 40% (3.3 mL, 29 mmol), was added, and the mixture was cooled to 0 °C. To the obtained solution, NH_3(aq), 25% (9.0 mL, 132 mmol), was added dropwise with constant stirring for 4 h. The mixture was brought to room temperature and left overnight to produce an orange-brown solution. The volatiles were removed on a rotary evaporator, and the obtained solid was dissolved in $CHCl_3$ (50 mL), dried over $MgSO_4$, filtered, and purified by column chromatography on silica gel, using $CHCl_3$ as the eluent. The intense yellow opaque band was collected. The yield of the oven-dried (8 h, 80 °C) ligand was 2.3 g (39%). ^{1}H NMR (300 MHz, DMSO-d_6): δ 13.40 (1H, s br, NH), 8.52 (1H, d, J = 8.5 Hz, CH^7), 8.41 (1H, d, J = 8.5 Hz, CH^8), 8.39 (1H, d, J = 8.2 Hz, CH^4), 7.93 (2H, s br, CH^{5,6}), 7.68 (1H, d, J = 8.2 Hz, CH^3), 7.30 (2H, s br, imH), 2.84 (3H, s, CH_3). ^{13}C NMR (100 MHz, $CDCl_3$): δ 159.20, 148.85, 146.81, 144.77, 137.78, 137.44, 128.30, 127.46, 126.62, 126.10, 124.60, 119.85, 56.51, 24.99, 18.98. Anal. Calcd for $C_{16}H_{12}N_4$: C, 73.83; H, 4.65; N, 21.52. Found: C, 73.58; H, 4.87; N, 21.47.

Complex [Fe(neoim)$_2$] (D). To a solution of neoimH (1000 mg, 3.8 mmol) in MeOH (20 mL) was added $Fe(BF_4)_2{\cdot}6H_2O$ (640 mg, 1.9 mmol). The resulting dark red solution was refrigerated (4 °C) overnight, and the plate-like red crystals that formed were filtered off, air-dried, and suspended in a mixture of NH_3(aq), 25% (30 mL), and $CHCl_3$ (100 mL). The violet-colored organic layer was separated, and the aqueous phase was extracted three more times with $CHCl_3$ (in portions of 50 mL each). The organic solutions were combined, dried over $MgSO_4$, and evaporated to dryness, producing a brown powder of the complex. The yield was 910 mg, 79%. Anal. Calcd for $C_{34}H_{28}FeN_8$: C, 67.56; H, 4.67; N, 18.54. Found: C, 67.25; H, 4.93; N, 18.18.

Complex [Fe(neoim)$_2$]·H$_2$O·2CHCl$_3$. Aiming at characterizing the neutral complexes through X-ray diffraction studies, single crystals of the H_2O−$CHCl_3$ solvate were obtained by slow diffusion of hexane vapors into solutions of [Fe(neoim)$_2$], obtained by dissolving microcrystalline samples (100 mg) in boiling chloroform (7 mL). The [Fe(neoim)$_2$]·H_2O·2$CHCl_3$ compound was obtained as dark-green block single crystals. Anal. Calcd for $C_{36}H_{32}Cl_6FeN_8O$: C, 50.20; H, 3.75; N, 13.01. Found: C, 49.88; H, 3.98; N, 13.44.

Physical Characterization. *Magnetic Measurements.* Magnetic measurements were performed on crystalline samples (20−40 mg) with a Quantum Design MPMS-XL-5 SQUID magnetometer working in the 2−400 K temperature range with an applied magnetic field of 1 T. Experimental susceptibilities were corrected for diamagnetism of the constituent atoms by the use of Pascal's constants.

Infrared Spectra. The solid-state absorption IR spectrum was recorded with an Agilent Technologies Cary 630-FTIR spectrometer equipped with a diamond micro-ATR accessory in the 4000−400 cm^{-1} range.

X-ray Powder Diffraction. X-ray powder diffraction (XRPD) measurements were performed on a PANalytical Empyrean X-ray powder diffractometer (monochromatic Cu Kα radiation) in capillary measurement mode.

Thermogravimetric Analysis. Thermogravimetric analysis was performed on a Mettler Toledo TGA/SDTA 851e, in the 290−800 K temperature range under a nitrogen atmosphere with a rate of 10 K min^{-1}.

Elemental Analyses. Elemental analyses (C, H, and N) were performed with a CE Instruments EA 1110 CHNS elemental analyzer.

Single-Crystal X-ray Measurements. Single crystals were mounted on a glass fiber using viscous hydrocarbon oil to coat the crystal and then transferred directly to the cold nitrogen stream for data collection. X-ray data were collected on a Supernova diffractometer equipped with a graphite monochromated Enhance (Mo) X-ray source (λ = 0.71073 Å). The program CrysAlisPro, Oxford Diffraction Ltd., was used for unit cell determination and data reduction. Empirical absorption correction was performed using spherical harmonics implemented in the SCALE3 ABSPACK scaling algorithm. The structures were solved by direct methods using SHELXS-2014 and refined by full matrix least-squares on F^2 using SHELXL-2014.[80] Non-hydrogen atoms were refined anisotropically, and hydrogen atoms were placed in calculated positions refined by using idealized geometries (riding model) and assigned fixed isotropic displacement parameters. CCDC 2260043 contains the supplementary crystallographic data for this paper. These data can be obtained free of charge from The Cambridge Crystallographic Data Centre via www.ccdc.cam.ac.uk/data_request/cif.

Sublimation of Thin Films. Thin films were sublimed under HV by heating the desolvated bulk powder of the [Fe(neoim)$_2$] molecule, priorly submitted to a degassing protocol (120 °C under 10^{-8} mbar pressure), under the conditions indicated above in the results description. This was performed within a customized CREATEC Molecular Beam Epitaxy system placed in a Clean Room Class 10,000. All prepared films had their thickness verified by means of profilometry using a KLA Alpha-Step D-500 instrument with nanometric resolution.

Optical Microscopy. OM imaging was performed by using a Nikon Eclipse LV-150N microscope coupled to a Nikon DS-FI3 camera and through a 50× objective.

Atomic Force Microscopy. AFM images were collected using a Bruker Dimension Icon with Scan Assyst in tapping mode and processed and analyzed using the Gwyddion program. The statistical value of roughness was calculated using this software as the rms value.

Infrared Spectroscopy. IR spectrum was collected using a Fourier transformation-infrared spectrometer NICOLET 5700 from Thermo Electron Corporation equipped with a module that allows for measuring the transmittance of the reflected IR light from a film sample between 3100 and 650 cm^{-1} and specifically grown on a 3 cm × 3 cm Au-coated glass substrate.

Raman Spectroscopy. Raman spectra were collected separately on a film grown on a SiO_2 substrate and on the bulk powder directly scattered on a glass slide using the same equipment and acquisition parameters, Horiba LabRAM HR Evolution equipped with a 473 nm laser beam with a maximum power of 1.08 mW·μm^{-2} and in the 1000−1700 cm^{-1} Raman shift region.

X-ray Absorption Spectroscopy. XAS characterization on the different films of [Fe(neoim)$_2$], indicated in the Results and Discussion section (deposited on 7 mm × 3 mm Si/SiO_2 substrates), and the desolvated bulk powder was performed at the Boreas beamline in ALBA synchrotron during both granted beamtimes and in-house experiments. The substrates supporting these films were fixed to copper sample holders using aluminum clips and placed on pieces of indium foil for their proper thermalization. The bulk powder

https://doi.org/10.1021/acs.chemmater.3c01704
Chem. Mater. 2023, 35, 9591−9602

was directly scattered onto C-tape stripes attached to a copper sample holder. For each case, the measurements implied the collection of three consecutive energy scans (for averaging) at each of a series of different temperatures within the range of 2−370 K in separately cooling and heating modes and focused at the Fe $L_{2,3}$ edge region. The scans were performed using total electron yield mode with a low photon flux (0.020 nA ≤ intensity ≤ 0.025 nA) and only exposing the samples to X-rays during the scan collection periods. For the LIESST effect studies, the samples were irradiated with a red laser [He−Ne LASER from Research Electro-optics Inc. (R-30993), wavelength 633 nm and power 12 mW] at 2 K, right after the cooling process and for only 10 min. This power corresponds to the output of the laser. The real power reaching the film cannot be ascertained since calibrating such magnitude presents vast technical difficulties inside the HV chamber of the beamline at the synchrotron, especially considering the time schedule limitations during an XAS experiment. All collected spectra for this study were processed for their analysis through background subtraction and normalization using the Igor program. The dependence of the HS fraction (%) with temperature for each case was calculated from a fitting to a linear combination of the spectra showing the characteristic shapes for (approximately) the full HS and the full LS fractions of the bulk material (370 K during heating and 80 K during cooling, respectively).

■ ASSOCIATED CONTENT

Supporting Information

The Supporting Information is available free of charge at https://pubs.acs.org/doi/10.1021/acs.chemmater.3c01704.

Room-temperature infrared spectra and experimental X-ray diffraction patterns for solvated and desolvated [Fe(neoim)$_2$] bulk powders, thermogravimetric analysis of the desolvated [Fe(neoim)$_2$] bulk powder, XAS results for an additional experiment performed on a 150 nm thick film of [Fe(neoim)$_2$], plots showing the fittings for the calculation of the HS fraction (γ_{HS}) from the XAS spectra for each sample at each temperature, and details of the crystal data collection and refinement parameters for [Fe(neoim)$_2$]·H_2O·$CHCl_3$ (PDF)

Accession Codes

CCDC 2260043 contains the supplementary crystallographic data for this article.

■ AUTHOR INFORMATION

Corresponding Authors

Maksym Seredyuk − *Instituto de Ciencia Molecular, Universidad de Valencia, Paterna 46980, Spain; Department of Chemistry, Taras Shevchenko National University of Kyiv, Kyiv 01601, Ukraine*; Email: maksym.seredyuk@knu.ua

José Antonio Real − *Instituto de Ciencia Molecular, Universidad de Valencia, Paterna 46980, Spain;* orcid.org/0000-0002-2302-561X; Email: jose.a.real@uv.es

Eugenio Coronado − *Instituto de Ciencia Molecular, Universidad de Valencia, Paterna 46980, Spain;* orcid.org/0000-0002-1848-8791; Email: eugenio.coronado@uv.es

Authors

Miguel Gavara-Edo − *Instituto de Ciencia Molecular, Universidad de Valencia, Paterna 46980, Spain;* orcid.org/0000-0002-0311-3874

Francisco Javier Valverde-Muñoz − *Instituto de Ciencia Molecular, Universidad de Valencia, Paterna 46980, Spain;* orcid.org/0000-0003-3578-5445

M. Carmen Muñoz − *Departamento de Fisica Aplicada, Universitat Politècnica de València, Valencia 46022, Spain;* orcid.org/0000-0003-2630-3897

Safaa Elidrissi Moubtassim − *Instituto de Ciencia Molecular, Universidad de Valencia, Paterna 46980, Spain;* orcid.org/0000-0002-6687-3854

Francisco Marques-Moros − *Instituto de Ciencia Molecular, Universidad de Valencia, Paterna 46980, Spain;* orcid.org/0000-0001-8199-5326

Javier Herrero-Martín − *CELLS-ALBA Synchrotron, Cerdanyola del Vallès 08290, Spain;* orcid.org/0000-0003-1986-8128

Kateryna Znovjyak − *Department of Chemistry, Taras Shevchenko National University of Kyiv, Kyiv 01601, Ukraine*

Complete contact information is available at: https://pubs.acs.org/10.1021/acs.chemmater.3c01704

Author Contributions

All authors have given approval to the final version of the manuscript.

Funding

The authors acknowledge the financial support from the European Union (ERC AdG Mol-2D 788222 and HORIZON-EIC-2022-Pathfinderopen-01 4D-NMR 101099676), the Spanish MICINN (2D-HETEROS PID2020-117152RB-100, cofinanced by FEDER, SPINCROSMAT PID2019-106147GB-I00 funded by MCIN/AEI/10.13039/501100011033 and Excellence Unit "María de Maeztu", CEX2019-000919-M), the Generalitat Valenciana (Prometeo program PROMETEO/2021/022), and the Ministry of Education and Science of Ukraine (grant nos. 22BF037-03 and 22BF037-04).

Notes

The authors declare no competing financial interest.

■ ACKNOWLEDGMENTS

M.G.-E. acknowledges the support of a fellowship FPU15/01474 from MIU. F.J.V.-M. acknowledges the support of the Generalitat Valenciana (APOSTD/2021/359). S.E.M. acknowledges the support of the Generalitat Valenciana with a Santiago Grisolía fellowship (GRISOLIAP/2018/046). All XAS experiments were performed at Boreas beamline at ALBA Synchrotron with J.H.-M. in both proposal and in-house experiments. The authors thank Alejandra Soriano Portillo and Ángel López Muñoz for their technical support.

■ REFERENCES

(1) Gütlich, P.; Goodwin, H. A. *Spin Crossover in Transition Metal Compounds I*; Gütlich, P., Goodwin, H. A., Eds.; *Topics in Current Chemistry*; Springer Berlin Heidelberg: Berlin, Heidelberg, 2004; Vol. *233*.

(2) Gütlich, P.; Goodwin, H. A. *Spin Crossover in Transition Metal Compounds II*; *Topics in Current Chemistry*; Springer Berlin Heidelberg: Berlin, Heidelberg, 2004; Vol. *234*.

(3) Gütlich, P.; Goodwin, H. A. *Spin Crossover in Transition Metal Compounds III*; *Topics in Current Chemistry*; Springer Berlin Heidelberg: Berlin, Heidelberg, 2004; Vol. *235*.

(4) König, E. Nature and Dynamics of the Spin-State Interconversion in Metal Complexes. *Complex Chemistry*; *Structure and Bonding*; Springer: Berlin, Heidelberg, 1991; Vol. *76*, pp 51−152.

(5) Gütlich, P.; Hauser, A.; Spiering, H. Thermal and Optical Switching of Iron(II) Complexes. *Angew. Chem., Int. Ed.* **1994**, *33* (20), 2024−2054.
(6) Real, J. A.; Gaspar, A. B.; Niel, V.; Muñoz, M. Communication between Iron(II) Building Blocks in Cooperative Spin Transition Phenomena. *Coord. Chem. Rev.* **2003**, *236* (1−2), 121−141.
(7) Real, J. A.; Gaspar, A. B.; Muñoz, M. C. Thermal, Pressure and Light Switchable Spin-Crossover Materials. *Dalton Trans.* **2005**, No. 12, 2062.
(8) Bousseksou, A.; Molnár, G.; Salmon, L.; Nicolazzi, W. Molecular Spin Crossover Phenomenon: Recent Achievements and Prospects. *Chem. Soc. Rev.* **2011**, *40* (6), 3313.
(9) Nicolazzi, W.; Bousseksou, A. Thermodynamical Aspects of the Spin Crossover Phenomenon. *C. R. Chim.* **2018**, *21* (12), 1060−1074.
(10) Molnár, G.; Rat, S.; Salmon, L.; Nicolazzi, W.; Bousseksou, A. Spin Crossover Nanomaterials: From Fundamental Concepts to Devices. *Adv. Mater.* **2018**, *30* (5), 1703862.
(11) Kumar, K. S.; Ruben, M. Sublimable Spin-Crossover Complexes: From Spin-State Switching to Molecular Devices. *Angew. Chem., Int. Ed.* **2021**, *60* (14), 7502−7521.
(12) Ekanayaka, T. K.; Hao, G.; Mosey, A.; Dale, A. S.; Jiang, X.; Yost, A. J.; Sapkota, K. R.; Wang, G. T.; Zhang, J.; N'Diaye, A. T.; Marshall, A.; Cheng, R.; Naeemi, A.; Xu, X.; Dowben, P. A. Nonvolatile Voltage Controlled Molecular Spin-State Switching for Memory Applications. *Magnetochemistry* **2021**, *7* (3), 37.
(13) Coronado, E. Molecular Magnetism: From Chemical Design to Spin Control in Molecules, Materials and Devices. *Nat. Rev. Mater.* **2020**, *5* (2), 87−104.
(14) Trofimenko, S. Boron-Pyrazole Chemistry. IV. Carbon- and Boron-Substituted Poly[(1-Pyrazolyl) Borates]. *J. Am. Chem. Soc.* **1967**, *89* (24), 6288−6294.
(15) Jesson, J. P.; Weiher, J. F.; Trofimenko, S. Mössbauer and Magnetic Susceptibility Investigation of the 5 T 2 - 1 A 1 Crossover in Some Octahedral Ferrous Complexes in the Solid State. *J. Chem. Phys.* **1968**, *48* (5), 2058−2066.
(16) Rat, S.; Ridier, K.; Vendier, L.; Molnár, G.; Salmon, L.; Bousseksou, A. Solvatomorphism and structural-spin crossover property relationship in bis[hydrotris(1,2,4-triazol-1-yl)borate]iron-(ii). *CrystEngComm* **2017**, *19* (24), 3271−3280.
(17) Ossinger, S.; Näther, C.; Buchholz, A.; Schmidtmann, M.; Mangelsen, S.; Beckhaus, R.; Plass, W.; Tuczek, F. Spin Transition of an Iron(II) Organoborate Complex in Different Polymorphs and in Vacuum-Deposited Thin Films: Influence of Cooperativity. *Inorg. Chem.* **2020**, *59* (12), 7966−7979.
(18) Grunwald, J.; Torres, J.; Buchholz, A.; Näther, C.; Kämmerer, L.; Gruber, M.; Rohlf, S.; Thakur, S.; Wende, H.; Plass, W.; Kuch, W.; Tuczek, F. Defying the inverse energy gap law: a vacuum-evaporable Fe(ii) low-spin complex with a long-lived LIESST state. *Chem. Sci.* **2023**, *14* (26), 7361−7380.
(19) Gakiya-Teruya, M.; Jiang, X.; Le, D.; Üngör, Ö.; Durrani, A. J.; Koptur-Palenchar, J. J.; Jiang, J.; Jiang, T.; Meisel, M. W.; Cheng, H.-P.; Zhang, X.-G.; Zhang, X.-X.; Rahman, T. S.; Hebard, A. F.; Shatruk, M. Asymmetric Design of Spin-Crossover Complexes to Increase the Volatility for Surface Deposition. *J. Am. Chem. Soc.* **2021**, *143* (36), 14563−14572.
(20) Atzori, M.; Poggini, L.; Squillantini, L.; Cortigiani, B.; Gonidec, M.; Bencok, P.; Sessoli, R.; Mannini, M. Thermal and Light-Induced Spin Transition in a Nanometric Film of a New High-Vacuum Processable Spin Crossover Complex. *J. Mater. Chem. C* **2018**, *6* (33), 8885−8889.
(21) Real, J. A.; Muñoz, M. C.; Faus, J.; Solans, X. Spin Crossover in Novel Dihydrobis(1-Pyrazolyl)Borate [H 2 B(Pz) 2]-Containing Iron(II) Complexes. Synthesis, X-Ray Structure, and Magnetic Properties of [FeL{H 2 B(Pz) 2} 2] (L = 1,10-Phenanthroline and 2,2′-Bipyridine). *Inorg. Chem.* **1997**, *36* (14), 3008−3013.
(22) Moliner, N.; Salmon, L.; Capes, L.; Muñoz, M. C.; Létard, J. F.; Bousseksou, A.; Tuchagues, J.-P.; McGarvey, J. J.; Dennis, A. C.; Castro, M.; Burriel, R.; Real, J. A. Thermal and Optical Switching of Molecular Spin States in the {[FeL[H 2 B(Pz) 2] 2} Spin-Crossover System (L = Bpy, Phen). *J. Phys. Chem. B* **2002**, *106* (16), 4276−4283.
(23) Thompson, A. L.; Goeta, A. E.; Real, J. A.; Galet, A.; Carmen Muñoz, M. Thermal and light induced polymorphism in iron(ii) spin crossover compounds. *Chem. Commun.* **2004**, *4* (12), 1390−1391.
(24) Ossinger, S.; Kipgen, L.; Naggert, H.; Bernien, M.; Britton, A. J.; Nickel, F.; Arruda, L. M.; Kumberg, I.; Engesser, T. A.; Golias, E.; Näther, C.; Tuczek, F.; Kuch, W. Effect of Ligand Methylation on the Spin-Switching Properties of Surface-Supported Spin-Crossover Molecules. *J. Phys.: Condens. Matter* **2020**, *32* (11), 114003.
(25) Rösner, B.; Milek, M.; Witt, A.; Gobaut, B.; Torelli, P.; Fink, R. H.; Khusniyarov, M. M. Reversible Photoswitching of a Spin-Crossover Molecular Complex in the Solid State at Room Temperature. *Angew. Chem., Int. Ed.* **2015**, *54* (44), 12976−12980.
(26) Ossinger, S.; Naggert, H.; Kipgen, L.; Jasper-Toennies, T.; Rai, A.; Rudnik, J.; Nickel, F.; Arruda, L. M.; Bernien, M.; Kuch, W.; Berndt, R.; Tuczek, F. Vacuum-Evaporable Spin-Crossover Complexes in Direct Contact with a Solid Surface: Bismuth versus Gold. *J. Phys. Chem. C* **2017**, *121* (2), 1210−1219.
(27) Naggert, H.; Rudnik, J.; Kipgen, L.; Bernien, M.; Nickel, F.; Arruda, L. M.; Kuch, W.; Näther, C.; Tuczek, F. Vacuum-Evaporable Spin-Crossover Complexes: Physicochemical Properties in the Crystalline Bulk and in Thin Films Deposited from the Gas Phase. *J. Mater. Chem. C* **2015**, *3* (30), 7870−7877.
(28) Gavara-Edo, M.; Valverde-Muñoz, F. J.; Córdoba, R.; Muñoz, M. C.; Herrero-Martín, J.; Real, J. A.; Coronado, E. Sublimable Complexes with Spin Switching: Chemical Design, Processing as Thin Films and Integration in Graphene-Based Devices. *J. Mater. Chem. C* **2023**, *11* (24), 8107−8120.
(29) Koenig, E.; Madeja, K. 5T2−1A1 Equilibriums in Some Iron(II)-Bis(1,10-Phenanthroline) Complexes. *Inorg. Chem.* **1967**, *6* (1), 48−55.
(30) Baker, W. A.; Bobonich, H. M. Magnetic Properties of Some High-Spin Complexes of Iron(II). *Inorg. Chem.* **1964**, *3* (8), 1184−1188.
(31) Gallois, B.; Real, J. A.; Hauw, C.; Zarembowitch, J. Structural Changes Associated with the Spin Transition in Bis(Isothiocyanato)-Bis(1,10-Phenanthroline)Iron: A Single-Crystal x-Ray Investigation. *Inorg. Chem.* **1990**, *29* (6), 1152−1158.
(32) Bernien, M.; Wiedemann, D.; Hermanns, C. F.; Krüger, A.; Rolf, D.; Kroener, W.; Müller, P.; Grohmann, A.; Kuch, W. Spin Crossover in a Vacuum-Deposited Submonolayer of a Molecular Iron(II) Complex. *J. Phys. Chem. Lett.* **2012**, *3* (23), 3431−3434.
(33) Rohlf, S.; Gruber, M.; Flöser, B. M.; Grunwald, J.; Jarausch, S.; Diekmann, F.; Kalläne, M.; Jasper-Toennies, T.; Buchholz, A.; Plass, W.; Berndt, R.; Tuczek, F.; Rossnagel, K. Light-Induced Spin Crossover in an Fe(II) Low-Spin Complex Enabled by Surface Adsorption. *J. Phys. Chem. Lett.* **2018**, *9* (7), 1491−1496.
(34) Kuroda-Sowa, T.; Yu, Z.; Senzaki, Y.; Sugimoto, K.; Maekawa, M.; Munakata, M.; Hayami, S.; Maeda, Y. Abrupt Spin Transitions and LIESST Effects Observed in Fe II Spin-Crossover Complexes with Extended π-Conjugated Schiff-Base Ligands Having N 4 O 2 Donor Sets. *Chem. Lett.* **2008**, *37* (12), 1216−1217.
(35) Thakur, S.; Golias, E.; Kumberg, I.; Senthil Kumar, K.; Hosseinifar, R.; Torres-Rodríguez, J.; Kipgen, L.; Lotze, C.; Arruda, L. M.; Luo, C.; Radu, F.; Ruben, M.; Kuch, W. Thermal- and Light-Induced Spin-Crossover Characteristics of a Functional Iron(II) Complex at Submonolayer Coverage on HOPG. *J. Phys. Chem. C* **2021**, *125* (25), 13925−13932.
(36) Kipgen, L.; Bernien, M.; Ossinger, S.; Nickel, F.; Britton, A. J.; Arruda, L. M.; Naggert, H.; Luo, C.; Lotze, C.; Ryll, H.; Radu, F.; Schierle, E.; Weschke, E.; Tuczek, F.; Kuch, W. Evolution of Cooperativity in the Spin Transition of an Iron(II) Complex on a Graphite Surface. *Nat. Commun.* **2018**, *9* (1), 2984.
(37) Bernien, M.; Naggert, H.; Arruda, L. M.; Kipgen, L.; Nickel, F.; Miguel, J.; Hermanns, C. F.; Krüger, A.; Krüger, D.; Schierle, E.; Weschke, E.; Tuczek, F.; Kuch, W. Highly Efficient Thermal and Light-Induced Spin-State Switching of an Fe(II) Complex in Direct Contact with a Solid Surface. *ACS Nano* **2015**, *9* (9), 8960−8966.

https://doi.org/10.1021/acs.chemmater.3c01704
Chem. Mater. 2023, 35, 9591−9602

(38) Poggini, L.; Milek, M.; Londi, G.; Naim, A.; Poneti, G.; Squillantini, L.; Magnani, A.; Totti, F.; Rosa, P.; Khusniyarov, M. M.; Mannini, M. Room temperature control of spin states in a thin film of a photochromic iron(ii) complex. *Mater. Horiz.* **2018**, *5* (3), 506−513.
(39) Shi, S.; Schmerber, G.; Arabski, J.; Beaufrand, J.-B.; Kim, D. J.; Boukari, S.; Bowen, M.; Kemp, N. T.; Viart, N.; Rogez, G.; Beaurepaire, E.; Aubriet, H.; Petersen, J.; Becker, C.; Ruch, D. Study of Molecular Spin-Crossover Complex Fe(Phen)2(NCS)2 Thin Films. *Appl. Phys. Lett.* **2009**, *95* (4), 043303.
(40) Kelai, M.; Tauzin, A.; Railean, A.; Repain, V.; Lagoute, J.; Girard, Y.; Rousset, S.; Otero, E.; Mallah, T.; Boillot, M.-L.; Enachescu, C.; Bellec, A. Interface versus Bulk Light-Induced Switching in Spin-Crossover Molecular Ultrathin Films Adsorbed on a Metallic Surface. *J. Phys. Chem. Lett.* **2023**, *14* (7), 1949−1954.
(41) Gavara-Edo, M.; Córdoba, R.; Valverde-Muñoz, F. J.; Herrero-Martín, J.; Real, J. A.; Coronado, E. Electrical Sensing of the Thermal and Light-Induced Spin Transition in Robust Contactless Spin-Crossover/Graphene Hybrid Devices. *Adv. Mater.* **2022**, *34* (33), 2202551.
(42) Kelai, M.; Repain, V.; Tauzin, A.; Li, W.; Girard, Y.; Lagoute, J.; Rousset, S.; Otero, E.; Sainctavit, P.; Arrio, M.-A.; Boillot, M.-L.; Mallah, T.; Enachescu, C.; Bellec, A. Thermal Bistability of an Ultrathin Film of Iron(II) Spin-Crossover Molecules Directly Adsorbed on a Metal Surface. *J. Phys. Chem. Lett.* **2021**, *12* (26), 6152−6158.
(43) Bairagi, K.; Iasco, O.; Bellec, A.; Kartsev, A.; Li, D.; Lagoute, J.; Chacon, C.; Girard, Y.; Rousset, S.; Miserque, F.; Dappe, Y. J.; Smogunov, A.; Barreteau, C.; Boillot, M. L.; Mallah, T.; Repain, V. Molecular-Scale Dynamics of Light-Induced Spin Cross-over in a Two-Dimensional Layer. *Nat. Commun.* **2016**, *7*, 12212.
(44) Shalabaeva, V.; Rat, S.; Manrique-Juarez, M. D.; Bas, A.-C.; Vendier, L.; Salmon, L.; Molnár, G.; Bousseksou, A. Vacuum Deposition of High-Quality Thin Films Displaying Spin Transition near Room Temperature. *J. Mater. Chem. C* **2017**, *5* (18), 4419−4425.
(45) Kipgen, L.; Bernien, M.; Tuczek, F.; Kuch, W. Spin-Crossover Molecules on Surfaces: From Isolated Molecules to Ultrathin Films. *Adv. Mater.* **2021**, *33* (24), 2008141.
(46) Gruber, M.; Berndt, R. Spin-Crossover Complexes in Direct Contact with Surfaces. *Magnetochemistry* **2020**, *6* (3), 35.
(47) Torres-Cavanillas, R.; Gavara-Edo, M.; Coronado, E. Bistable Spin-crossover Nanoparticles for Molecular Electronics. *Adv. Mater.* **2023**, 2307718.
(48) Konstantinov, N.; Tauzin, A.; Noumbé, U. N.; Dragoe, D.; Kundys, B.; Majjad, H.; Brosseau, A.; Lenertz, M.; Singh, A.; Berciaud, S.; Boillot, M.-L.; Doudin, B.; Mallah, T.; Dayen, J.-F. Electrical Read-out of Light-Induced Spin Transition in Thin Film Spin Crossover/Graphene Heterostructures. *J. Mater. Chem. C* **2021**, *9* (8), 2712−2720.
(49) Decurtins, S.; Gütlich, P.; Köhler, C.; Spiering, H.; Hauser, A. Light-Induced Excited Spin State Trapping in a Transition-Metal Complex: The Hexa-1-Propyltetrazole-Iron (II) Tetrafluoroborate Spin-Crossover System. *Chem. Phys. Lett.* **1984**, *105* (1), 1−4.
(50) Létard, J. F.; Guionneau, P.; Rabardel, L.; Howard, J. A. K.; Goeta, A. E.; Chasseau, D.; Kahn, O. Structural, Magnetic, and Photomagnetic Studies of a Mononuclear Iron(II) Derivative Exhibiting an Exceptionally Abrupt Spin Transition. Light-Induced Thermal Hysteresis Phenomenon. *Inorg. Chem.* **1998**, *37* (17), 4432−4441.
(51) Hauser, A. Intersystem Crossing in Fe(II) Coordination Compounds. *Coord. Chem. Rev.* **1991**, *111* (2), 275−290.
(52) Hauser, A.; Vef, A.; Adler, P. Intersystem Crossing Dynamics in Fe(II) Coordination Compounds. *J. Chem. Phys.* **1991**, *95* (12), 8710−8717.
(53) Hauser, A.; Enachescu, C.; Daku, M. L.; Vargas, A.; Amstutz, N. Low-Temperature Lifetimes of Metastable High-Spin States in Spin-Crossover and in Low-Spin Iron(II) Compounds: The Rule and Exceptions to the Rule. *Coord. Chem. Rev.* **2006**, *250* (13−14), 1642−1652.
(54) Collison, D.; Garner, C. D.; McGrath, C. M.; Mosselmans, J. F. W.; Roper, M. D.; Seddon, J. M. W.; Sinn, E.; Young, N. A. Soft X-Ray Induced Excited Spin State Trapping and Soft X-Ray Photochemistry at the Iron L2,3 Edge in [Fe(Phen)2(NCS)2] and [Fe(Phen)2(NCSe)2] (Phen = 1,10-Phenanthroline). *J. Chem. Soc., Dalton Trans.* **1997**, *2* (22), 4371−4376.
(55) Yazdani, S.; Phillips, J.; Ekanayaka, T. K.; Cheng, R.; Dowben, P. A. The Influence of the Substrate on the Functionality of Spin Crossover Molecular Materials. *Molecules* **2023**, *28* (9), 3735.
(56) Zhang, X.; N'Diaye, A. T.; Jiang, X.; Zhang, X.; Yin, Y.; Chen, X.; Hong, X.; Xu, X.; Dowben, P. A. Indications of Magnetic Coupling Effects in Spin Cross-over Molecular Thin Films. *Chem. Commun.* **2018**, *54* (8), 944−947.
(57) Ekanayaka, T. K.; Kurz, H.; McElveen, K. A.; Hao, G.; Mishra, E.; N'Diaye, A. T.; Lai, R. Y.; Weber, B.; Dowben, P. A. Evidence for surface effects on the intermolecular interactions in Fe(ii) spin crossover coordination polymers. *Phys. Chem. Chem. Phys.* **2022**, *24* (2), 883−894.
(58) Zhang, X.; Costa, P. S.; Hooper, J.; Miller, D. P.; N'Diaye, A. T.; Beniwal, S.; Jiang, X.; Yin, Y.; Rosa, P.; Routaboul, L.; Gonidec, M.; Poggini, L.; Braunstein, P.; Doudin, B.; Xu, X.; Enders, A.; Zurek, E.; Dowben, P. A. Locking and Unlocking the Molecular Spin Crossover Transition. *Adv. Mater.* **2017**, *29* (39), 1702257.
(59) Jiang, X.; Hao, G.; Wang, X.; Mosey, A.; Zhang, X.; Yu, L.; Yost, A. J.; Zhang, X.; DiChiara, A. D.; N'Diaye, A. T.; Cheng, X.; Zhang, J.; Cheng, R.; Xu, X.; Dowben, P. A. Tunable Spin-State Bistability in a Spin Crossover Molecular Complex. *J. Phys.: Condens. Matter* **2019**, *31* (31), 315401.
(60) Naggert, H.; Bannwarth, A.; Chemnitz, S.; von Hofe, T.; Quandt, E.; Tuczek, F. First Observation of Light-Induced Spin Change in Vacuum Deposited Thin Films of Iron Spin Crossover Complexes. *Dalton Trans.* **2011**, *40* (24), 6364.
(61) Davesne, V.; Gruber, M.; Studniarek, M.; Doh, W. H.; Zafeiratos, S.; Joly, L.; Sirotti, F.; Silly, M. G.; Gaspar, A. B.; Real, J. A.; Schmerber, G.; Bowen, M.; Weber, W.; Boukari, S.; Da Costa, V.; Arabski, J.; Wulfhekel, W.; Beaurepaire, E. Hysteresis and Change of Transition Temperature in Thin Films of Fe{[Me 2 Pyrz] 3 BH} 2, a New Sublimable Spin-Crossover Molecule. *J. Chem. Phys.* **2015**, *142* (19), 194702.
(62) Rubio-Giménez, V.; Bartual-Murgui, C.; Galbiati, M.; Núñez-López, A.; Castells-Gil, J.; Quinard, B.; Seneor, P.; Otero, E.; Ohresser, P.; Cantarero, A.; Coronado, E.; Real, J. A.; Mattana, R.; Tatay, S.; Martí-Gastaldo, C. Effect of Nanostructuration on the Spin Crossover Transition in Crystalline Ultrathin Films. *Chem. Sci.* **2019**, *10* (14), 4038−4047.
(63) Bartual-Murgui, C.; Rubio-Giménez, V.; Meneses-Sánchez, M.; Valverde-Muñoz, F. J.; Tatay, S.; Martí-Gastaldo, C.; Muñoz, M. C.; Real, J. A. Epitaxial Thin-Film vs Single Crystal Growth of 2D Hofmann-Type Iron(II) Materials: A Comparative Assessment of Their Bi-Stable Spin Crossover Properties. *ACS Appl. Mater. Interfaces* **2020**, *12* (26), 29461.
(64) Lefter, C.; Rat, S.; Costa, J. S.; Manrique-Juárez, M. D.; Quintero, C. M.; Salmon, L.; Séguy, I.; Leichle, T.; Nicu, L.; Demont, P.; Rotaru, A.; Molnár, G.; Bousseksou, A. Current Switching Coupled to Molecular Spin-States in Large-Area Junctions. *Adv. Mater.* **2016**, *28* (34), 7508−7514.
(65) Schleicher, F.; Studniarek, M.; Kumar, K. S.; Urbain, E.; Katcko, K.; Chen, J.; Frauhammer, T.; Hervé, M.; Halisdemir, U.; Kandpal, L. M.; Lacour, D.; Riminucci, A.; Joly, L.; Scheurer, F.; Gobaut, B.; Choueikani, F.; Otero, E.; Ohresser, P.; Arabski, J.; Schmerber, G.; Wulfhekel, W.; Beaurepaire, E.; Weber, W.; Boukari, S.; Ruben, M.; Bowen, M. Linking Electronic Transport through a Spin Crossover Thin Film to the Molecular Spin State Using X-Ray Absorption Spectroscopy Operando Techniques. *ACS Appl. Mater. Interfaces* **2018**, *10* (37), 31580−31585.
(66) Poggini, L.; Gonidec, M.; Canjeevaram Balasubramanyam, R. K.; Squillantini, L.; Pecastaings, G.; Caneschi, A.; Rosa, P.

https://doi.org/10.1021/acs.chemmater.3c01704
Chem. Mater. 2023, 35, 9591−9602

Temperature-Induced Transport Changes in Molecular Junctions Based on a Spin Crossover Complex. *J. Mater. Chem. C* **2019**, *7* (18), 5343−5347.
(67) Gopakumar, T. G.; Bernien, M.; Naggert, H.; Matino, F.; Hermanns, C. F.; Bannwarth, A.; Mühlenberend, S.; Krüger, A.; Krüger, D.; Nickel, F.; Walter, W.; Berndt, R.; Kuch, W.; Tuczek, F. Spin-Crossover Complex on Au(111): Structural and Electronic Differences Between Mono- and Multilayers. *Chem.—Eur. J.* **2013**, *19* (46), 15702−15709.
(68) Ludwig, E.; Naggert, H.; Kalläne, M.; Rohlf, S.; Kröger, E.; Bannwarth, A.; Quer, A.; Rossnagel, K.; Kipp, L.; Tuczek, F. Iron(II) Spin-Crossover Complexes in Ultrathin Films: Electronic Structure and Spin-State Switching by Visible and Vacuum-UV Light. *Angew. Chem., Int. Ed.* **2014**, *53* (11), 3019−3023.
(69) Palamarciuc, T.; Oberg, J. C.; El Hallak, F.; Hirjibehedin, C. F.; Serri, M.; Heutz, S.; Létard, J. F.; Rosa, P. Spin Crossover Materials Evaporated under Clean High Vacuum and Ultra-High Vacuum Conditions: From Thin Films to Single Molecules. *J. Mater. Chem.* **2012**, *22* (19), 9690.
(70) Gopakumar, T. G.; Matino, F.; Naggert, H.; Bannwarth, A.; Tuczek, F.; Berndt, R. Electron-Induced Spin Crossover of Single Molecules in a Bilayer on Gold. *Angew. Chem., Int. Ed.* **2012**, *51* (25), 6262−6266.
(71) Pronschinske, A.; Chen, Y.; Lewis, G. F.; Shultz, D. A.; Calzolari, A.; Buongiorno Nardelli, M.; Dougherty, D. B. Modification of Molecular Spin Crossover in Ultrathin Films. *Nano Lett.* **2013**, *13* (4), 1429−1434.
(72) Pronschinske, A.; Bruce, R. C.; Lewis, G.; Chen, Y.; Calzolari, A.; Buongiorno-Nardelli, M.; Shultz, D. A.; You, W.; Dougherty, D. B. Iron(Ii) Spin Crossover Films on Au(111): Scanning Probe Microscopy and Photoelectron Spectroscopy. *Chem. Commun.* **2013**, *49* (89), 10446.
(73) Warner, B.; Oberg, J. C.; Gill, T. G.; El Hallak, F.; Hirjibehedin, C. F.; Serri, M.; Heutz, S.; Arrio, M.-A.; Sainctavit, P.; Mannini, M.; Poneti, G.; Sessoli, R.; Rosa, P. Temperature- and Light-Induced Spin Crossover Observed by X-Ray Spectroscopy on Isolated Fe(II) Complexes on Gold. *J. Phys. Chem. Lett.* **2013**, *4* (9), 1546−1552.
(74) Dugay, J.; Aarts, M.; Giménez-Marqués, M.; Kozlova, T.; Zandbergen, H. W.; Coronado, E.; van der Zant, H. S. J. Phase Transitions in Spin-Crossover Thin Films Probed by Graphene Transport Measurements. *Nano Lett.* **2017**, *17* (1), 186−193.
(75) Torres-Cavanillas, R.; Morant-Giner, M.; Escorcia-Ariza, G.; Dugay, J.; Canet-Ferrer, J.; Tatay, S.; Cardona-Serra, S.; Giménez-Marqués, M.; Galbiati, M.; Forment-Aliaga, A.; Coronado, E. Spin-Crossover Nanoparticles Anchored on MoS2 Layers for Heterostructures with Tunable Strain Driven by Thermal or Light-Induced Spin Switching. *Nat. Chem.* **2021**, *13* (11), 1101−1109.
(76) van Geest, E. P.; Shakouri, K.; Fu, W.; Robert, V.; Tudor, V.; Bonnet, S.; Schneider, G. F. Contactless Spin Switch Sensing by Chemo-Electric Gating of Graphene. *Adv. Mater.* **2020**, *32* (10), 1903575.
(77) Boix-Constant, C.; García-López, V.; Navarro-Moratalla, E.; Clemente-León, M.; Zafra, J. L.; Casado, J.; Guinea, F.; Mañas-Valero, S.; Coronado, E. Strain Switching in van Der Waals Heterostructures Triggered by a Spin-Crossover Metal-Organic Framework. *Adv. Mater.* **2022**, *34* (11), 2110027.
(78) Dayen, J.-F.; Konstantinov, N.; Palluel, M.; Daro, N.; Kundys, B.; Soliman, M.; Chastanet, G.; Doudin, B. Room Temperature Optoelectronic Devices Operating with Spin Crossover Nanoparticles. *Mater. Horiz.* **2021**, *8* (8), 2310−2315.
(79) Shaul, M.; Cohen, Y. Novel Phenanthroline-Containing Trinuclear Double-Stranded Helicates: Self-Recognition between Helicates with Phenanthroline and Bipyridine Binding Sites. *J. Org. Chem.* **1999**, *64* (26), 9358−9364.
(80) Sheldrick, G. M. Crystal Structure Refinement with SHELXL. *Acta Crystallogr., Sect. C: Struct. Chem.* **2015**, *71* (1), 3−8.

https://doi.org/10.1021/acs.chemmater.3c01704
Chem. Mater. 2023, 35, 9591−9602